

Electronic Supplementary Information (ESI)

High adsorptive properties of covalent triazine-based frameworks (CTFs) for surfactants from aqueous solution

Asamanjoy Bhunia^a, Subarna Dey^a, Maria Bous^b, Chenyang Zhang^b, Wolfgang von Rybinski^{b*} and Christoph Janiak^{a*}

^aInstitut für Anorganische Chemie und Strukturchemie, Heinrich-Heine-Universität Düsseldorf, 40204 Düsseldorf, Germany. Fax: +49-211-81-12287; Tel: +49-211-81-12286.

^bInstitute for Physical Chemistry and Electrochemistry, Heinrich-Heine-Universität Düsseldorf, 40204 Düsseldorf, Germany. Fax: +49-211-81-12803; Tel: +49-211-81-14867.

* Corresponding author: E-mail: vonRybinski@uni-duesseldorf.de, janiak@uni-duesseldorf.de;

Other Emails:

asamanjoy.bhuniam@gmail.com

subarna.dey@uni-duesseldorf.de

maria.bous@uni-duesseldorf.de

chenyang.zhang@uni-duesseldorf.de

1. Experimental Section

Materials and methods

All chemicals were purchased from commercial suppliers (Sigma-Aldrich, Acros Organics, and Alfa Aesar chemical company) and used without further purification, unless stated otherwise.

Infrared (IR) spectra were obtained on a Bruker FT-IR Tensor 37 Spectrometer in the 4000-550 cm⁻¹ region with 2 cm⁻¹ resolution as KBr disks. Elemental (CNH) analyses were carried out with a PerkinElmer 2400 series 2 elemental analyzer. Powder X-ray diffraction (PXRD) data was collected on a Bruker D2 Phaser diffractometer using a flat sample holder (also a flat silicon, low background sample holder) and Cu K α_1/α_2 radiation with $\lambda = 1.5418 \text{ \AA}$ at 30 kV covering 2 θ angles 5-80° over a time of 2 h, that is. 0.01°/sec. Diffractograms were obtained on flat layer sample holders where at low angle the beam spot is strongly broadened

so that only a fraction of the reflected radiation reaches the detector which leads to low relative intensities measured at $2\theta < 7^\circ$. For hygroscopic or air-sensitive samples, the sample holder can be sealed with a dome. Scanning electron microscopy (SEM) images were obtained using an ESEM Quanta 400 FEG SEM equipped with a secondary electron detector. Scanning electron microscopy images of CTF-1 after SDS adsorption (Fig. S5b) were obtained using a Jeol JSM-6510LV analyzer with LaB₆ cathode. Thermogravimetric analyses (TGA) were carried out at a ramp rate of 5 °C/min in a N₂ flow with a Netzsch Thermo-Microbalance Apparatus TG 209 F3 Tarsus.

Sorption isotherms were measured using a Micromeritics ASAP 2020 automatic gas sorption analyzer equipped with oil-free vacuum pumps (ultimate vacuum $<10^{-8}$ mbar) and valves, which guaranteed contamination free measurements. The sample was connected to the preparation port of the sorption analyzer and degassed under vacuum until the outgassing rate, i.e., the rate of pressure rise in the temporarily closed manifold with the connected sample tube, was less than 2 μ Torr/min at the specified temperature 200 °C. After weighing, the sample tube was then transferred to the analysis port of the sorption analyzer. All used gases (He, N₂, CO₂) were of ultra-high purity (UHP, grade 5.0, 99.999%) and the STP volumes are given according to the NIST standards (293.15 K, 101.325 kPa). Helium gas was used for the determination of the cold and warm free space of the sample tubes. N₂ sorption isotherms was measured at 77 K (liquid nitrogen bath), whereas CO₂ sorption isotherms was measured at 293 \pm 1 K (passive thermostating) and 273.15 K (ice/deionized water bath). The heat of adsorption values and the DFT pore size distributions ('N₂ DFT slit pore' model) were calculated out using the ASAP 2020 v3.05 software.

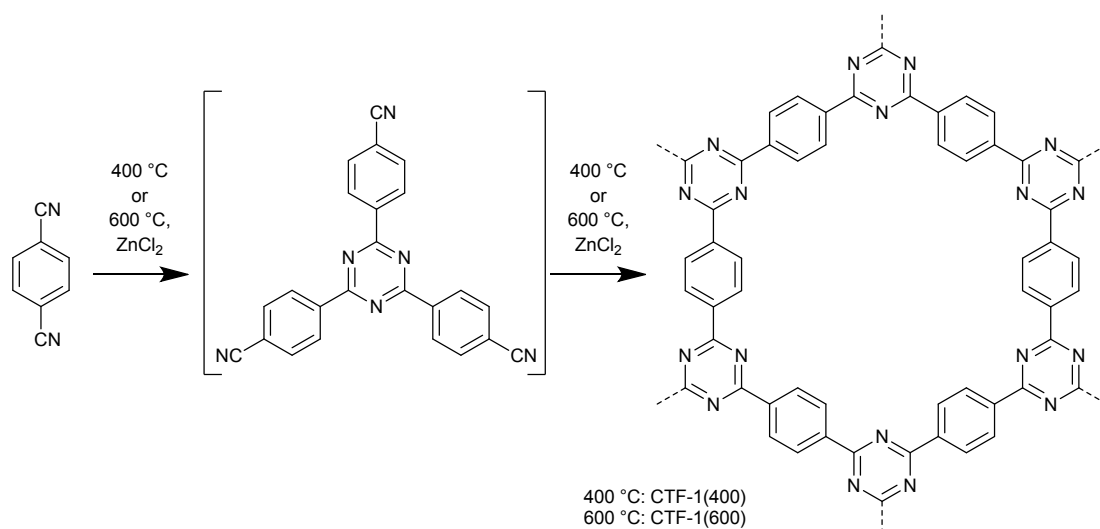
2. Synthesis

CTF-1(400) and CTF-1(600) were synthesized according to the literature procedure¹:

A mixture of 1,4-dicyanobenzene (1.28 g, 10 mmol) and anhydrous ZnCl₂ (6.8 g, 50 mmol) were placed into a quartz ampoule under inert conditions. The ampoule was evacuated, sealed and heated to 400 or 600 °C for 48 h followed by cooling to room temperature. The black product was collected and stirred with water for 72 h. Then the product was isolated by filtration and again stirred with 200 mL of 2 mol/L HCl for 24 h. The resulting black powder was further washed with water (3 \times 75 mL), THF (3 \times 75 mL), acetone (3 \times 75 mL) and dried in vacuum. Yield: 90 %.

For CTF-1(400): The monomer was heated at 400 °C.

For CTF-1(600): The monomer was heated at 600 °C.



Scheme 1. Synthesis of CTF-1 from 1,4-dicyanobenzene by using the ionothermal reaction with ZnCl₂ as porogen and catalyst at two different temperatures.

3. FT-IR Spectrum

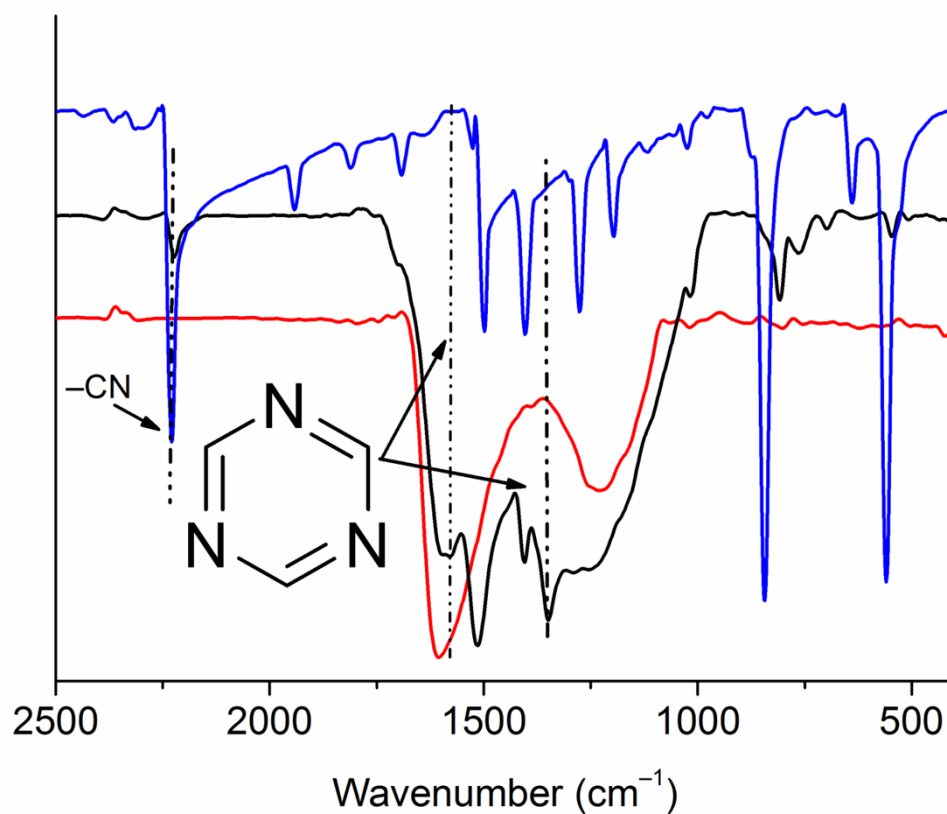


Fig. S1a: FT-IR spectrum of 1,4-dicyanobenzene (blue), CTF-1(400) (black) and CTF-1(600) (red) as synthesized before surfactant adsorption.

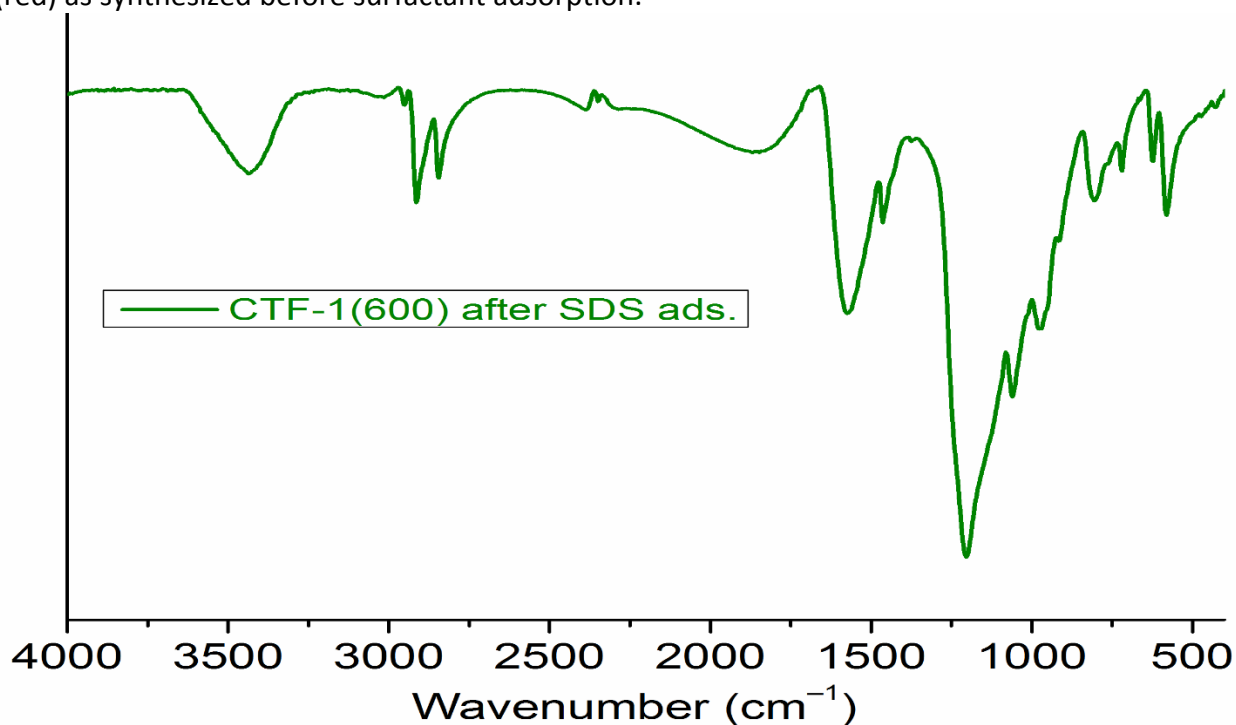


Fig. S1a: FT-IR spectrum of CTF-1(600) after SDS (sodium dodecylsulfate) surfactant adsorption at 20 mmol/L. Bands of SDS are superimposed on the CTF-1(600) bands. The characteristic band at 1570 cm^{-1} of CTF-1(600) in Fig. S1a is retained.

4. Powder X-ray diffraction patterns

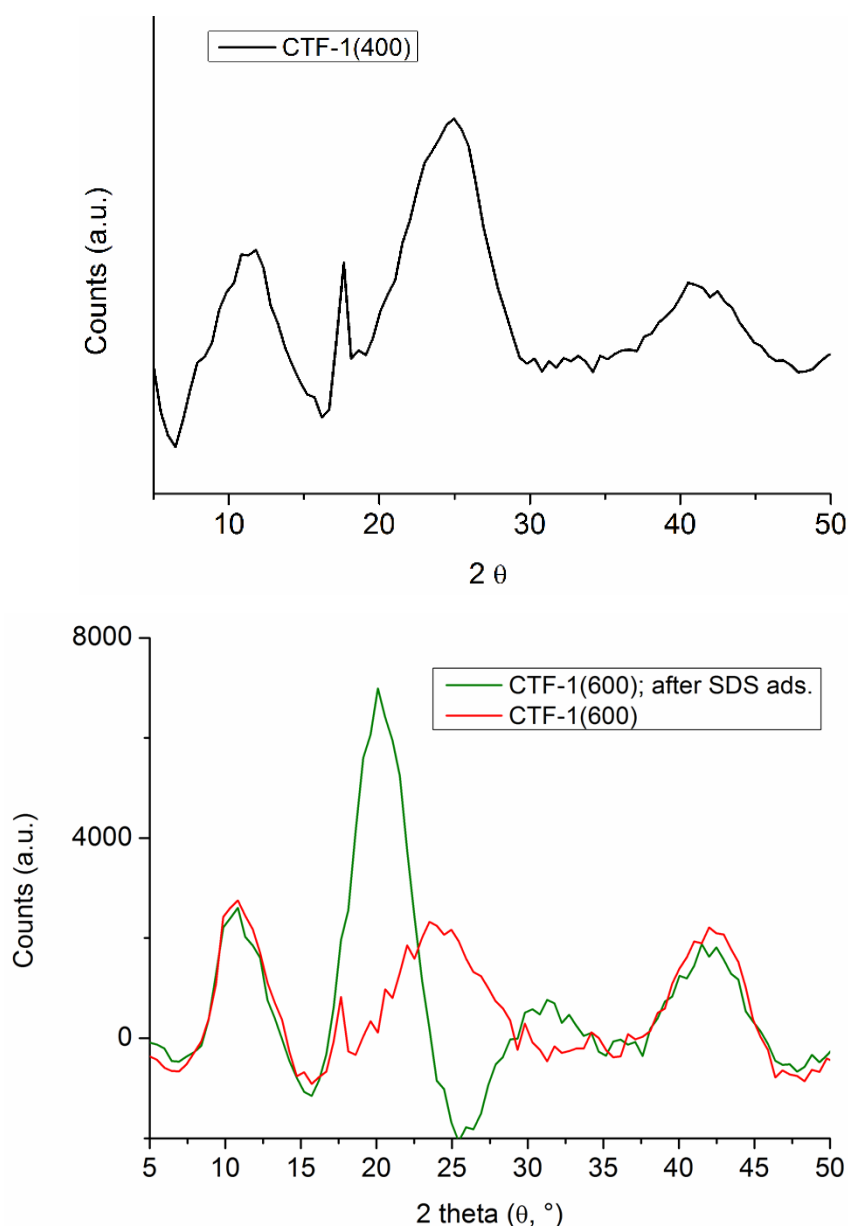


Fig. S2: Powder X-ray diffraction pattern of CTF-1(400) and CTF-1(600) before (*red*) and after SDS (sodium dodecylsulfate) surfactant adsorption at 20 mmol/L (*green*). The "crystallinity" of the CTF sample is retained albeit with shifts in the peak positions and changes in the relative intensities. The PXRD of CTF-1(600) after SDS has the peak shifted from 25° to 20° with increased intensity. In the work by Kuhn et al.² the broad peak at $2\theta = 26.1^\circ$ was assigned to the (001) peak and the distance of the (001) peak in the diffraction pattern was used for the layer distance between the triazine sheets ($c = 3.4 \text{ \AA}$). Here the shift of this peak with its maximum to $2\theta = 20.1^\circ$ indicates an increase of the layer distance between the triazine sheets to 4.4 \AA (according to $d = \lambda/2\sin\theta$ with $\lambda = 1.5418 \text{ \AA}$). Interlayer insertion of surfactants can also be observed for layer silicates such as Montmorillonite or Hectorite, which leads to an enhanced distance of the single layers of the solid.³

5. Elemental analysis

Compound	Temperature (°C)	Calculated (wt % and molar ratio)					Found (wt% and molar ratio)				
		C	H	N	C/H	C/N	C	H	N	C/H	C/N
CTF-1(400)	400	74.99	3.15	21.86	1.98	4.00	72.03	2.96	13.82	2.03	6.08
CTF-1(600)	600	74.99	3.15	21.86	1.98	4.00	68.13	2.14	8.91	2.7	8.92

6. Thermogravimetric analysis

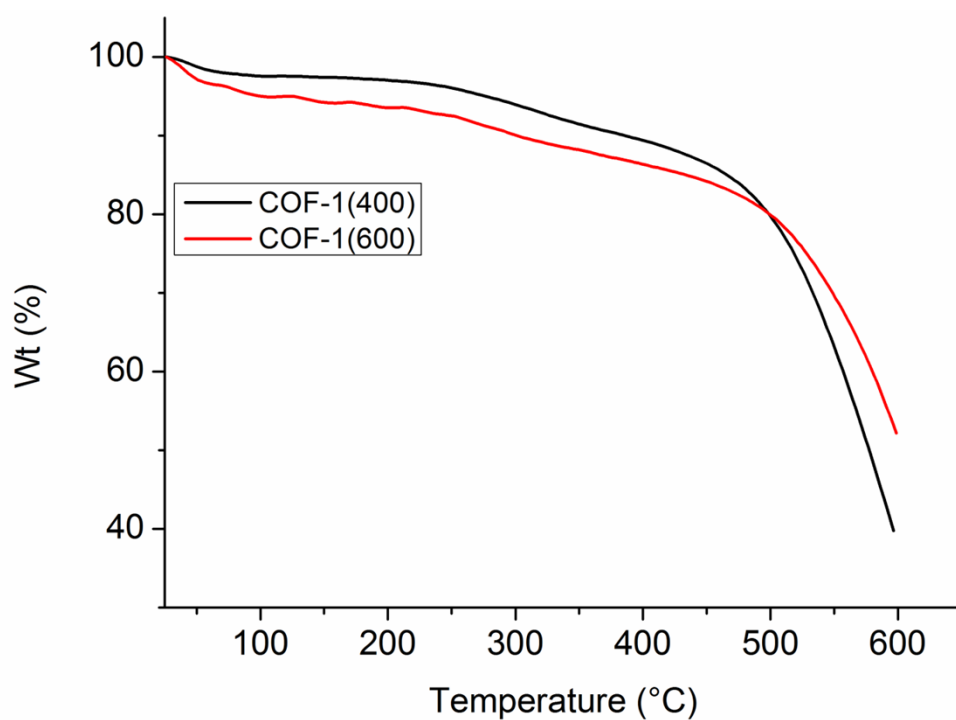


Fig. S3: Thermogravimetric analysis (TGA) data for CTF-1(400) and CTF-1(600).

7. Scanning electron micrographs (SEM) images

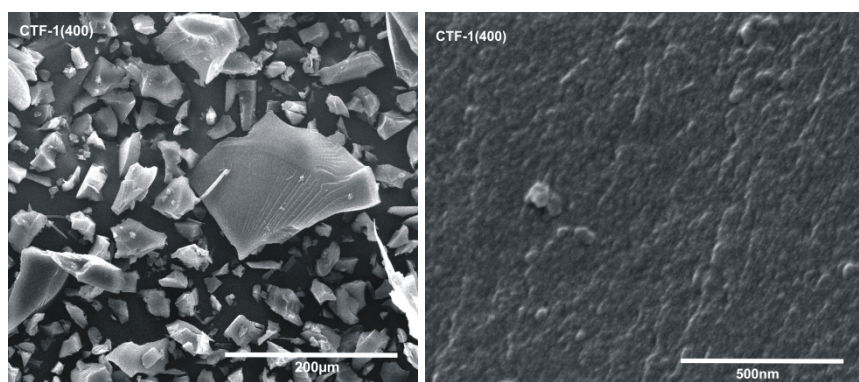


Fig. S4: SEM images for CTF-1(400) before surfactant adsorption.

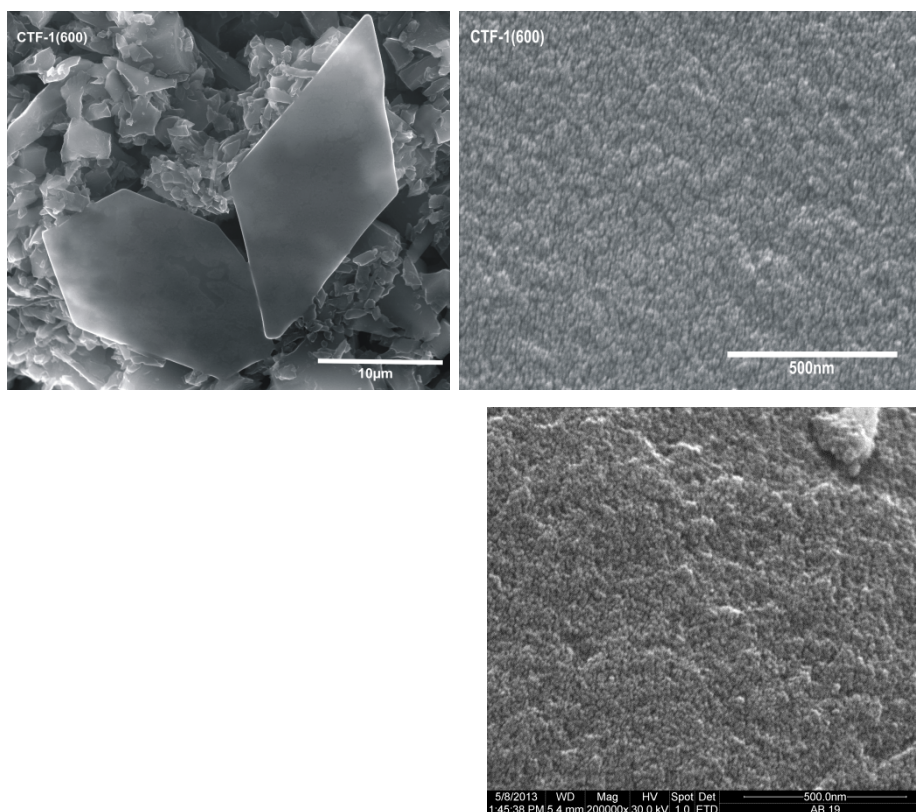


Fig. S5a: SEM images for CTF-1(600) before surfactant adsorption.

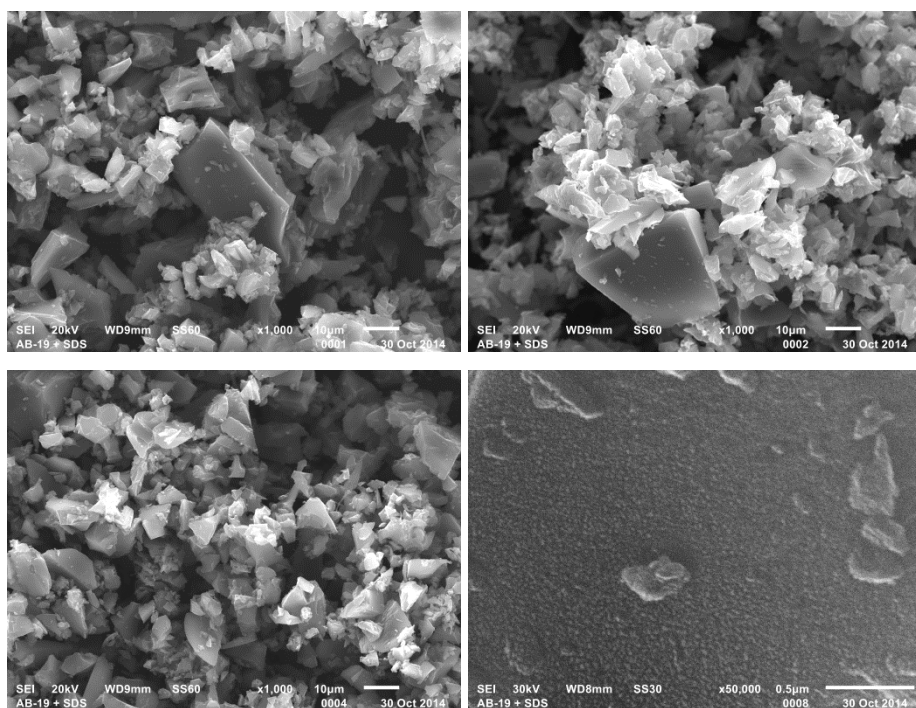


Fig. S5b: SEM images for CTF-1(600) after SDS (sodium dodecylsulfate) surfactant adsorption at an SDS equilibrium concentration of 20 mmol/L. There is no evident change in microscopic morphology after SDS adsorption.

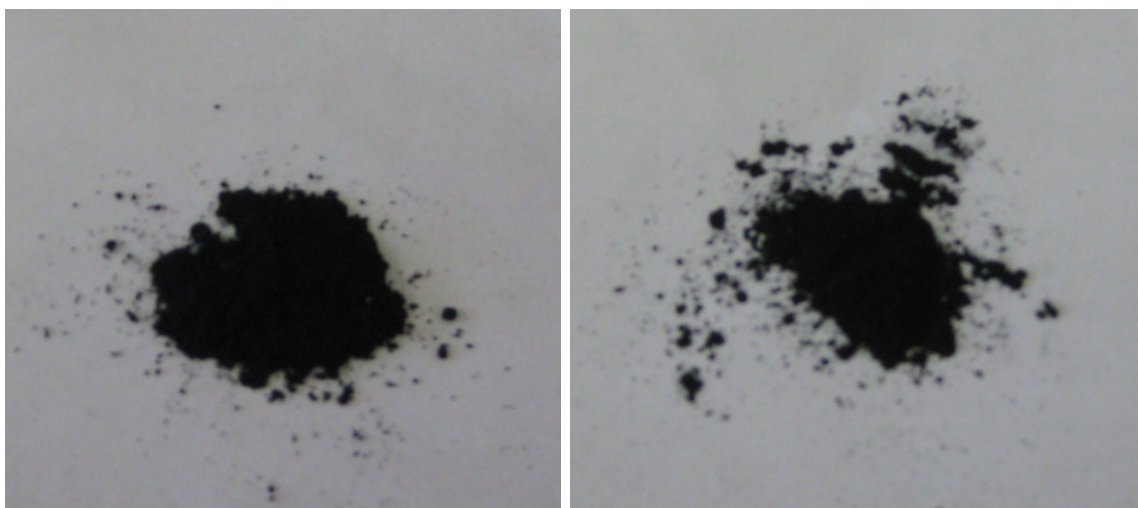


Fig. S5c: Camera photographs of CTF-1(600) before (left) after after SDS adsorption at an SDS equilibrium concentration of 20 mmol/L. The macroscopic black appearance did not change.

8. N₂ Sorption and pore size distribution:

N₂ sorption studies were performed to calculate the porosity. The surface area is calculated by applying the Brunauer–Emmett–Teller (BET) model over the pressure range of $P/P_0 = 0.01–0.05$. The measured BET surface areas are 970 for CTF-1(400) and and 1390 m²g⁻¹ CTF-1(600).

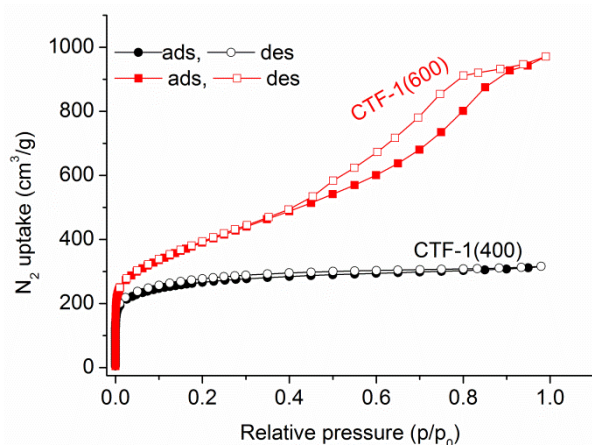


Fig. S6: Nitrogen adsorption-desorption isotherms for CTF-1(600) and CTF-1(400).

To understand the nature of porosity, non-local density functional theory (NLDFT) pore size distributions using a slit-pore model based on the N₂ adsorption isotherms were calculated. A narrow distribution of micropores centered mainly at 5, 6 and 12 Å were observed for CTF-

1(400) leading to small rings and cages associated with triazine formation (Fig. S7). On the other hand, micropores as well as mesopores were found for CTF-1(600).

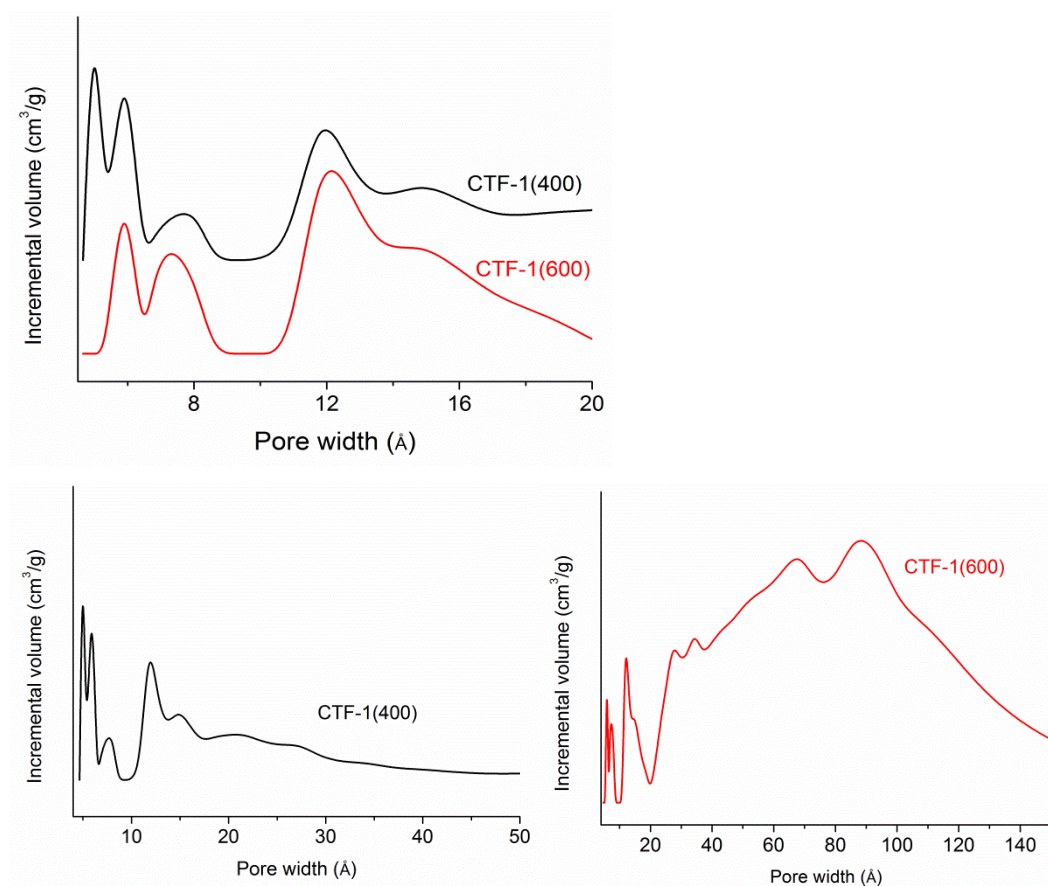


Fig. S7a: NL-DFT pore size distribution curve of CTF-1(400) and CTF-1(600).

Typically, the pore size distribution of a porous solid is evaluated from the analysis of N₂ adsorption isotherms measured at 77 K as was done above (Figure S6). However, that at such cryogenic temperature diffusion of N₂ molecules into carbon micropores is very slow. Moreover, diffusion limitations at this temperature might influence adsorption in ultramicropores (pores smaller than 7 Å).⁴ For porous carbons which usually contain a wide range of pore sizes including ultramicropores, this would require time-consuming N₂ adsorption measurements and may still lead to under-equilibration of measured adsorption isotherms, which will give erroneous results of the analysis. For porous carbons problem of this type can be eliminated by using CO₂ adsorption analysis at 273 K.⁵ The saturation pressure of CO₂ at 0°C is very high (~26141 Torr), therefore low relative pressure measurements necessary for the micropore analysis are achieved in the range of moderate

absolute pressures (1–760 Torr).⁶ At 273 K and under higher absolute pressures CO₂ molecules can more easily access ultramicropores than N₂ at ~77 K and the kinetic diameter of CO₂ (3.3 Å) is also a little bit smaller than for N₂ (3.64 Å). So, advantages for of CO₂ micropore analysis at 273 K versus N₂ analysis at 77 K are (i) faster analysis and (ii) greater confidence that measured adsorption points are equilibrated (both due to higher diffusion rates) and (iii) extension of the range of analysis to pores of smaller sizes that are accessible to CO₂ molecules but not to N₂.

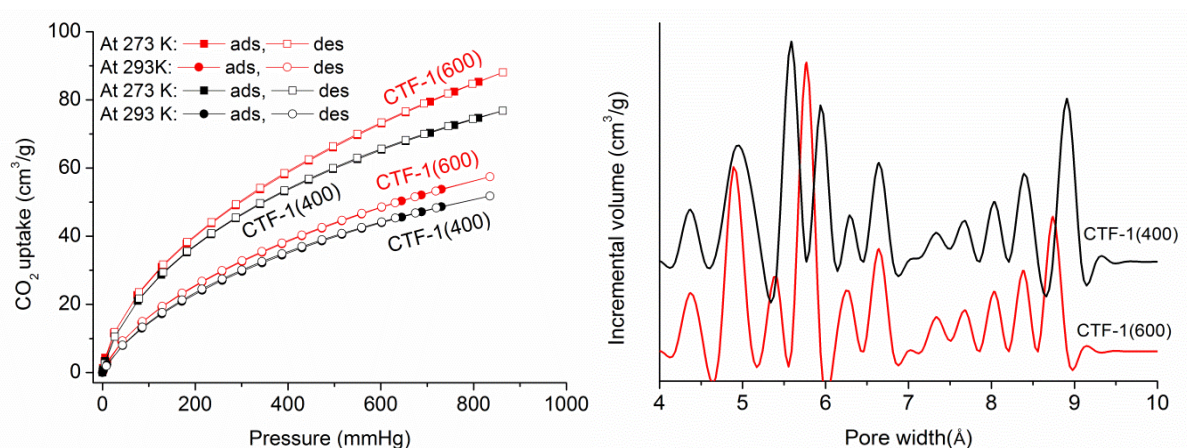


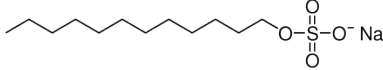
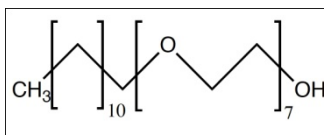
Fig. S7b: CO₂ sorption (left) and NLDFT pore size distribution (PSD) curve from CO₂ sorption (right).

Thus, from CO₂ adsorption isotherms at 273 K, the pore size distribution was derived between 4-10 Å by using NLDFT with a "CO₂ on carbon based slit-pore model" (Figure S7b). CO₂ adsorption with the NLDFT model yields a better resolved PSD towards the ultramicropore end than from N₂ adsorption isotherms. Both PSD values are very similar below 10 Å (1 nm) (Figure S7a and S7b). Moreover, we also studied the CO₂ uptake capacities for both the CTF-1(400) and CTF-1(600) as it is unknown until now. The CO₂ uptake capacities of CTF-1(400) and CTF-1(600) lie between 82 to 49 cm³ g⁻¹ (Figure S7b) which is comparable with the values for PCTFs from our previous work.⁷

9. Adsorption of surfactants

The surfactants for the adsorption studies from solution were sodium dodecylsulfate (SDS) and alkyl polyglycoether ($C_{12}EO_7$) (Table S1). The alkyl polyglycoether was a product with an alkyl chain distribution ranging from C_{12} to C_{18} and an average ethoxylation grade of 7.

Table S1: Surfactants used for the adsorption experiment from solution

Surfactant	Supplier	Structure	Purity
sodium dodecylsulfate (SDS)	Roth		$\geq 99,5 \%$
alkyl polyglycoether ($C_{12}EO_7$)	BASF		C_{12} main alkyl component (48 %) EO ₇ on average

General procedure for surfactant adsorption: A known amount of solid is mixed with a known concentrated surfactant solution with stirring for 1h followed by centrifugation to separate the supernatant. To calculate the amount of, e.g., SDS adsorbed on, e.g., CTF-1(600), we have determined the surface tension of the solution which correlates to the SDS equilibrium concentration from the calibration curve in Figure S8. No influence of the CTF on the surface tension of the aqueous solutions was observed.

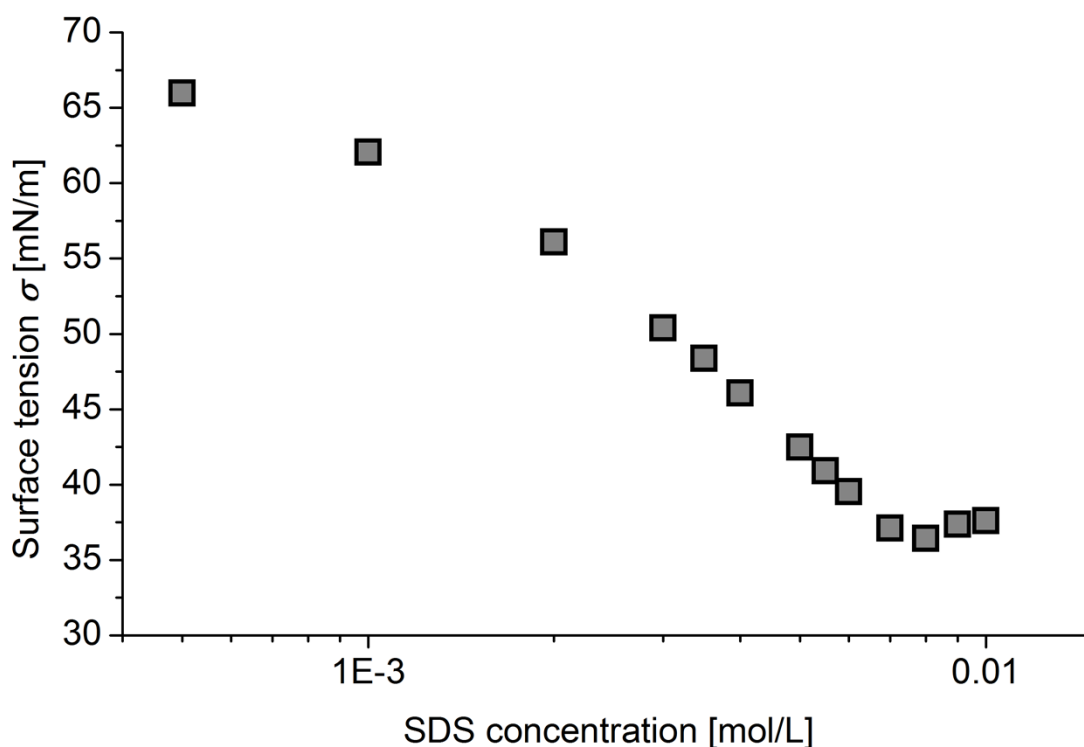


Fig. S8: Surface tension of sodium dodecylsulfate as a function of concentration

The graph in Figure S8 shows the typical surface activity of a surfactant in dependence of the concentration. At low concentrations the surface tension strongly decreases with the concentration, whereas above the critical micelle concentration (cmc) the surface tension remains nearly constant. The slight minimum close to the critical micelle concentration is caused by minor impurities of the surfactant. The linear decrease of surface tension with higher concentration below the cmc was used to calculate the adsorbed amounts on the CTFs. The adsorbed amounts of the surfactants from an aqueous solution on the solids were calculated according to equation S1:

$$\Gamma = \frac{\Delta c V}{m a_s} \quad (\text{S1})$$

where, Γ = adsorbed amounts ($\mu\text{mol m}^{-2}$); Δc = concentration difference before and after the adsorption (mmol L^{-1}); V = volume of the solution (L); m = mass of the adsorbent (g); a_s = specific surface area of the adsorbent ($\text{m}^2 \text{g}^{-1}$).

10. Possible arrangements of the adsorbed molecules on the surface of CTFs

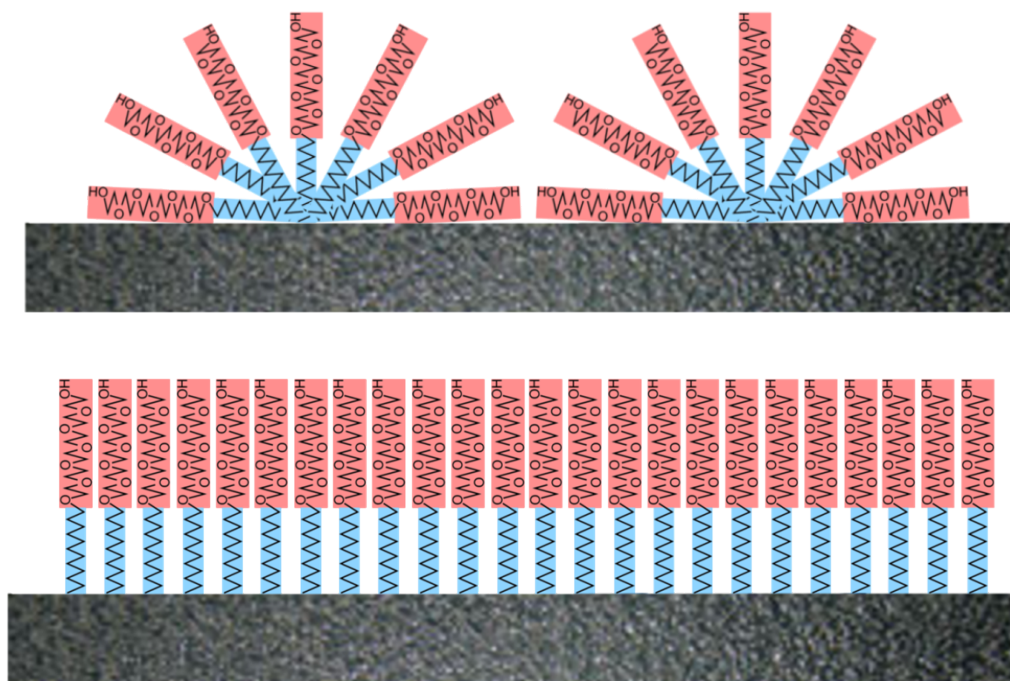


Fig. S9: Possible arrangements of the adsorbed molecules of SDS and $C_{12}EO_7$, respectively, on the surface of CTFs at low surfactant concentrations. Exemplary $C_{12}EO_7$ hemimicellar (top) and monolayer adsorption (bottom) on hydrophobic surface is shown here. The size ratio of hydrophilic head group (red) and hydrophobic tail (blue) is drawn to scale. The size of the sulfate head group of SDS is comparable to $C_{12}EO_7$ in diameter but shorter in length.

Surfactants can either adsorb via hydrogen bonding or electrostatic forces of the polar group to the polar groups of the solid surface or with the non-polar alkyl chain with the triazin ring structure via van der Waals forces like with carbon black surfaces.

Monolayers with horizontal and vertical orientation depending on the surface coverage or bilayers and admicelle and micelle structures are possible.^{3,8} As an example the sketch (Fig. S9) shows possible structures for the mentioned non-polar adsorption mechanism between the nonpolar part of the surfactant and the ring structure of the solid, forming close-packed monolayers at higher surface coverage and the hemimicellar structures.^{3,8,9}

In ref. 9 (ref. 15 in main article) it is suggested that for aromatic compounds the adsorption follows mainly "non-hydrophobic" mechanisms including hydrogen bonding (hydroxyl- and amino-substituted compounds), electrostatic attraction (anionized compounds), and π - π

electron-donor–acceptor (EDA) interaction (nitroaromatic compounds). In the case of surfactants on CTF we think that both non-hydrophobic and van-der-Waals force mechanisms are possible. In any case the adsorbed amounts should be similar for both mechanisms.³ Many references of the adsorption and adsorption mechanisms of different surfactant types on various surfaces are given in ref. 3.

A trimerization reaction of nitrile groups can construct triazine rings (see Scheme 1 in main text). Each triazine ring can act as a triangular node with phenyl rings and thereby built a continuous sheet or layer network. The resulting sheets can form a hexagonal lattice system with an eclipsed AAA structure where atoms of each layer are placed above their analogues in the next layer.²

Surfactants are amphiphilic compounds that adsorb at interfaces such as liquid/liquid, solid/liquid and gas/liquid systems. This is due to the fact that these compounds combine in their structure a non-polar part which is mainly a hydrocarbon alkyl chain containing 8 to 18 carbon atoms and a polar part, as the head-group which can be either from a non-ionic, an ionic (cationic or anionic) or a zwitterionic nature (see Table S1). By adsorption onto a solid surface, a surfactant can convert the surface from a hydrophobic species to a hydrophilic species and vice versa. In hydrophilic surfaces, surfactants can form the quasi two-dimensional admicelles similar to the aggregate structure, name as spherical or cylindrical micelles or bilayer structures.⁸ On the other hand, in hydrophobic surfaces, surfactant aggregates tend to form either monolayer or hemimicellar structure such as hemispherical or hemicylindrical (Fig. S9).¹⁰ However, the critical packing factor of the surfactant predicts the admicelles or hemicelles structure.¹¹

We note, however, that the surfactants (cf. Table S1) were not chosen with their particular properties to be adapted to the CTF-1 surface. Rather we chose common surfactants which are widely applied in the field.

1 P. Kuhn, A. I. Forget, D. Su, A. Thomas and M. Antonietti, *J. Am. Chem. Soc.*, 2008, **130**, 13333-13337

2 P. Kuhn, M. Antonietti and A. Thomas, *Angew. Chem. Int. Ed.*, 2008, **47**, 3450-3453.

3 B. Dobias, X. Qiu and W. von Rybinski, *Solid-Liquid Dispersions*, Surfactant Science Series, Marcel Dekker 1999.

4 F. Rodriguez-Reinoso and A. Linares-Solano, in *Chemistry and Physics of Carbon*, Vol. 21 (P. A. Thrower, Ed.) Marcel Dekker, New York, 1988.

5 J. Garrido, A. Linares-Solano, J. M. Martin-Martinez, M. Molina-Sabio, F. Rodriguez-Reinoso and R. Torregosa, *Langmuir*, 1987, **3**, 76; D. Cazorla-Amoros, J. Alcaniz-Monje and A. Linares-Solano, *Langmuir*, 1996, **12**, 2820; J. Garcia-Martinez and D. Cazorla-

-
- Amoros, A. Linares-Solano, in *Characterization of Porous Solids V* (K. K. Unger, G. Kreysa and J. P. Baselt, Eds.) Elsevier, Amsterdam, 2000, pp. 485-494.
- 6 Quantachrome Instruments (1900 Corporate Drive, Boynton Beach, FL 33426 USA, www.quantachrome.com) Powder Tech Note 35.
- 7 A. Bhunia, I. Boldog, A. Moller and C. Janiak, *J. Mater. Chem. A*, 2013, **1**, 14990–14999.
- 8 F. Tiberg, J. Brinck and L. Grant, Adsorption and surface-induced self-assembly of surfactants at the solid-aqueous interface, *Curr. Opin. J. Colloid Interface Sci.*, 2000, **4**, 411–419.
- 9 T. Wang, K. Kailasam, P. Xiao, G. Chen, L. Chen, L. Wang, J. Li and J. Zhu, *Microporous Mesoporous Mater.*, 2014, **187**, 63-70; J. Liu, H. Chen, S. Zheng and Z. Xu, *J. Chem. Eng. Data*, 2013, **58**, 3557–3562; J. Liu, E. Zong, H. Fu, S. Zheng, Z. Xu and D. Zhu, *J. Colloid Interface Sci.*, 2012, **372**, 99-107; W. Zhang, F. Liang, C. Li, L.-G. Qiu, Y.-P. Yuan, F.-M. Peng, X. Jiang, A.-J. Xie, Y.-H. Shen and J.-F. Zhu, *J. Hazardous Mater.*, 2011, **186**, 984-990.
- 10 S. Manne, J. P. Cleveland, H. E. Gaub, G. D. Stucky and P. K. Hansma, Direct visualization of surfactant hemimicelles by force microscopy of the electric double layer, *Langmuir*, 1994, **10**, 4409–4413.
- 11 M. J. Rosen, *Surfactants and Interfacial Phenomena*, 3rd ed., Wiley-Interscience, New Jersey, 2004, pp. 38–59.